



## Soot concentration and temperature measurements in co-annular, nonpremixed CH<sub>4</sub>/air laminar flames at pressures up to 4 MPa

Kevin A. Thomson<sup>a,\*</sup>, Ömer L. Gülder<sup>b</sup>, Elizabeth J. Weckman<sup>a</sup>, Roydon A. Fraser<sup>a</sup>, Greg J. Smallwood<sup>c</sup>, Dave R. Snelling<sup>c</sup>

<sup>a</sup> Mechanical Engineering Department, University of Waterloo, Waterloo, ON N2L 3G1, Canada

<sup>b</sup> Institute for Aerospace Studies, University of Toronto, Toronto, ON M3H 5T6, Canada

<sup>c</sup> National Research Council of Canada, ICPET, Combustion Research Lab, Building M-9, 1200 Montreal Road, Ottawa, ON K1A 0R6, Canada

Received 25 May 2004; received in revised form 30 November 2004; accepted 30 November 2004

Available online 4 January 2005

### Abstract

Laminar nonpremixed methane–air flames were studied over the pressure range of 0.5 to 4 MPa using a new high-pressure combustion chamber. Flame characterization showed very good flame stability over the range of pressures, with a flame tip *rms* flicker of less than 1% in flame height. At all pressures, soot was completely oxidized within the visible flame. Spectral soot emission (SSE) and line-of-sight attenuation (LOSA) measurements provided radially resolved measurements of soot volume fraction and soot temperature at pressures from 0.5 to 4.0 MPa. Such measurements provide an improved understanding of the influence of pressure on soot formation and have not been reported previously in laminar nonpremixed flames for pressures above 0.4 MPa. SSE and LOSA soot concentration values typically agree to within 30% and both methods exhibit similar trends in the spatial distribution of soot concentration. Maximum soot concentration depended on pressure according to a power law, where the exponent on pressure is about 2 for the range of pressures between 0.5 and 2.0 MPa, and about 1.2 for 2.0 to 4.0 MPa. Peak carbon conversion to soot also followed a power-law dependence on pressure, where the pressure exponent is unity for pressures between 0.5 and 2.0 MPa and 0.1 for 2.0 to 4.0 MPa. The pressure dependence of sooting propensity diminished at pressures above 2.0 MPa. Soot concentrations measured in this work, when transformed to line-integrated values, are consistent with the measurements of Flower and Bowman for pressures up to 1.0 MPa [Proc. Combust Inst. 21 (1986) 1115–1124] and Lee and Na for pressures up to 0.4 MPa [JSME Int. J. Ser. B 43 (2000) 550–555]. Soot temperature measurements indicate that the overall temperatures decrease with increasing pressure; however, the differences diminish with increasing height in the flame. Low down in the flame, temperatures are about 150 K lower at pressures of 4.0 MPa than those at 0.5 MPa. In the upper half of the flame the differences reduce to 50 K.

Crown Copyright © 2004 Published by Elsevier Inc. on behalf of The Combustion Institute. All rights reserved.

**Keywords:** Soot formation; High pressure; Laminar nonpremixed flame

\* Corresponding author. Fax: +1-613-957-7869.

E-mail address: [kevin.thomson@nrc.ca](mailto:kevin.thomson@nrc.ca) (K.A. Thomson).

## 1. Introduction

With increasing environmental and health awareness [1–3] and new legislation [4] on particulate emission, there is a need to reduce the soot emissions from practical combustion systems. Since most practical combustors operate at high pressures (i.e., 2–10 MPa) it is of interest to understand how pressure influences the combustion phenomena, in particular soot formation pathways. There have been a number of fundamental studies in this area using premixed flat flames, e.g., [5–7], counterflow diffusion flames, e.g., [8–11], and coflow nonpremixed flames, e.g., [12–15]; however, these studies have not comprehensively addressed the issue of soot formation at high pressures.

Using a nonpremixed flame burner operating with ethylene, Flower and Bowman [13] report that maximum line-of-sight integrated soot volume fractions depends on pressure to the  $n$ th power

$$f_{v_{\text{line}}} = \int f_v(r) dr \propto P^n, \quad (1)$$

where  $n = 1.2 \pm 0.1$  for  $P = 0.1$  to 1.0 MPa. Lee and Na [15] show similar trends in line-of-sight integrated soot volume fractions for pressures of 0.1 to 0.4 MPa in an ethylene laminar diffusion flame. Their measurements suggest  $n = 1.26$ . These results are difficult to interpret and/or apply in practical combustion situations, however, since they represent linearly weighted averages through an annular soot distribution. The only spatially resolved measurements of soot volume fraction as a function of pressure are reported by Lee and Na [15]. Their data are quite limited, but suggest  $f_{v_{\text{max}}} \propto P^2$  for  $P = 0.2$  to 0.4 MPa at a height of 20 mm above the burner nozzle, where  $f_{v_{\text{max}}}$  is the maximum soot volume fraction.

Flower [14] measured line-of-sight averaged soot temperatures in ethylene nonpremixed flames as a function of height at pressures of 0.1 to 0.7 MPa. Their plots typically show an initial high temperature at the base of the flame which drops off by  $z = 5$ –10 mm, followed by a region where the temperature levels or slowly climbs, and finally a zone in the upper half of the flame where the temperature decreases at a constant gradient with height. The temperature decrease at the top of the flame is linked to the cessation of soot oxidation which leads to smoking flames. From his plots, it is observed that the soot temperature drops with increasing pressure at all heights. Conversely, the increase of temperature in the lower to middle portion of the flame is enhanced by pressure, bringing the values of temperature measured at various pressures into closer agreement at about the mid height of the flames. Cessation of soot oxidation in the upper half of the flame made it impossible to

observe whether this trend would have continued, had the soot oxidation carried through to completion.

Information on soot formation processes in non-premixed laminar flames at higher pressures is very limited. This motivates the overall objective of the present research to investigate the relationships between pressure and soot formation in annular, non-premixed laminar methane flames. The main objective of the research reported in this paper is to experimentally determine spatially resolved soot volume fraction and temperature in flames at elevated pressures. Spectral soot emission (SSE) and line-of-sight attenuation (LOSA) measurements in the methane flame are presented for ambient pressures from 0.5 to 4.0 MPa. These results greatly extend any available information on flame sooting tendency as a function of pressure.

## 2. Methodology

The new experimental pressure vessel used in this study is designed for working pressures up to 10 MPa and for continuous flowthrough of combustion gases. This paper represents the first documented measurements in the new high-pressure flame facility. A schematic of the chamber is shown in Fig. 1. The chamber is large, with an internal height of 600 mm and an internal diameter of 240 mm. Physical access to the chamber is possible through the upper and lower flanges. Optical access into the chamber is possible through three viewing ports oriented so that line-of-sight and  $90^\circ$  scatter measurements are possible. The chamber is mounted on an external 3-axis translation system.

The nonpremixed annular flame burner built for this study is based on a design by Miller and Maahs [12] who achieved a stable flame over a pressure

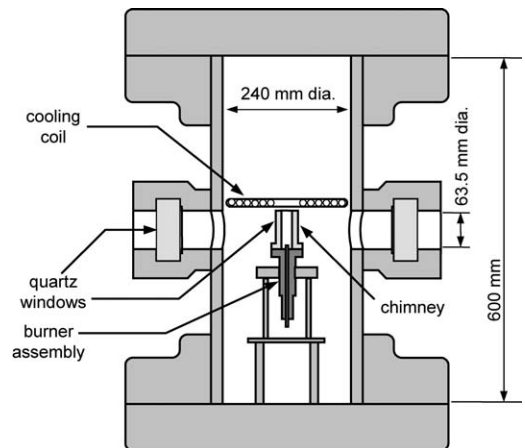


Fig. 1. Schematic of the high-pressure combustion chamber.

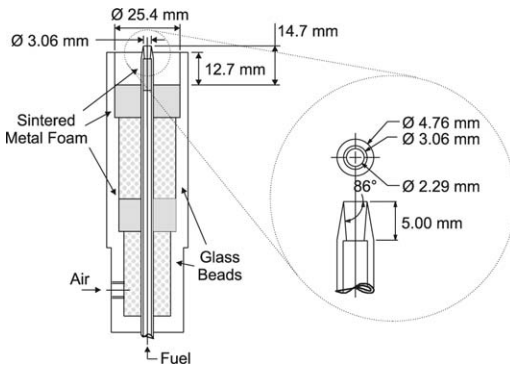


Fig. 2. Nonpremixed laminar coflow burner.

range of 0.1 to 5.0 MPa. A schematic of the burner used in the present study is included in Fig. 2. The burner has a fuel nozzle exit diameter of 3.06 mm and an air shroud diameter of 25 mm. Sintered metal foam elements (80 pores/inch) are included in the fuel and air nozzles to straighten and reduce instabilities in the flow and to create a top hat exit velocity profile as the gases leave the foam elements. A tapered fuel nozzle reduces recirculation from the burner tip and improves stability of the fluid–ambient interface [12]. In the original design, a cylindrical quartz tube surrounded the flame to aid flame stabilization. For the present experiments, the quartz tube was replaced by a new chimney designed to include three flat windows aligned with the three viewing ports on the chamber. The flame is ignited using a glow plug incorporated into the chimney and located above the flame. The fuel burned is methane.

In order to filter out water droplets formed in the flame exhaust and to prevent water condensation on the chamber viewing ports, a cooling coil is installed in the chamber, level with the top of the chimney and filling the area between the outside diameter of the chimney and the inside diameter of the chamber. All fluid moving from the upper to the lower portion of the chamber passes over the surface of the cooling coil. Water condenses out of the gas onto the coils and thereby is filtered from the ambient fluid. Nitrogen jets are also installed in the view ports to blow dry purge gas across the faces of the windows. Under steady-state operation, the flame heats the chimney windows sufficiently to prevent condensation.

During the flame visualization and stability experiments, methane flow rates of 0.55 and 0.66 mg/s were tested while the air flow rate was maintained at 0.4 g/s. Flame stability, at pressures of 0.1, 0.5, 1.0, 2.0, 4.0, 6.0, and 8.0 MPa, was monitored using a digital video camera. Fig. 3 includes single images of the flame at the above pressures for a methane flow rate of 0.66 mg/s. At pressures of 0.5 to 4.0 MPa, the flames exhibit good, long-term stability with an *rms* flicker of

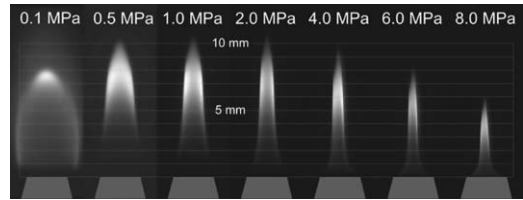


Fig. 3. Flame images at pressures from 0.1 to 8 MPa. The methane flow rate is 0.66 mg/s and the air flow rate is 0.4 g/s.

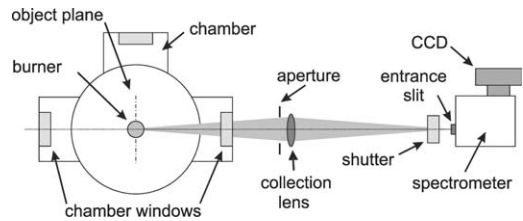


Fig. 4. Schematic of the spectral soot emission diagnostic.

the flame tip of less than 1% of the flame height. At pressures above 4.0 MPa the flames were not consistently stable and further work is required before soot studies can be performed at these high pressures.

The theory and overall experimental layout of the spectral soot emission diagnostic have been described previously [16]. In SSE, line-of-sight radiation emission from soot is measured along chords through the flame. A series of emission projections at a given height in the flame can be inverted to obtain radially resolved values of emission from which temperature and soot volume fraction can be determined when soot optical properties are known or assumed. A schematic of the SSE test apparatus is included in Fig. 4. For the present measurements a 300-mm focal length lens ( $f/45$ , 2:1 magnification) is used to image the object plane at the burner center onto the vertical entrance slit (height 500  $\mu\text{m}$ , width 25  $\mu\text{m}$ ) of a spectrometer. Output from the spectrometer is focused onto a 16-bit CCD detector (1100  $\times$  330 pixels). Knife-edge scans across a diffuse light source located at the object plane indicated a horizontal spatial resolution of 50  $\mu\text{m}$  over the depth of field defined by the burner nozzle exit diameter. The system is calibrated for radiation intensity using a calibrated filament lamp placed inside the chamber. Soot emission is measured over the wavelength range of 690–945 nm. Spectra are averaged over the height of the entrance slit as well as across 12 spectral regions, each 21 nm wide. This provides 12 adjacent spectral data points per line-of-sight acquisition. One-dimensional tomography is applied to each wavelength range using a three-point Abel inversion method [17]. Local temperatures are determined from the spectral shape of the inverted soot emission intensity. Soot volume fraction is

then determined from the soot emission intensity using the measured temperatures. Details of the method used to calculate temperature and soot volume fraction from line-of-sight transmissivity measurements are described in [16].

The soot refractive index function,  $E(m)$ , must be determined *ex situ* to the current experiment. For this, one of the best sources of information on refractive index can be found in the work of Faeth and co-workers (e.g., [18–20]) though there is considerable debate in the literature on this topic [21]. Krishnan et al. estimate an error on their measurements for  $E(m)_\lambda$  to be between 14 and 24% [20]. A linear regression to the  $E(m)_\lambda$  data points over the wavelength range of 488 to 800 nm indicates a nearly horizontal trend line with approximately 5%/μm variation in  $E(m)_\lambda$ . During initial development of the SSE diagnostic, SSE measurements of soot concentration and temperature were made in an atmospheric pressure nonpremixed flame and compared with 2D light attenuation soot concentration measurements and CARS temperature measurements. Results were analyzed for a variety of functional fits for  $E(m)_\lambda$  and it was determined that an  $E(m)_\lambda$  function independent of wavelength (i.e.,  $E(m)$  independent of wavelength) showed the best agreement [16]. It was also shown that a change in slope from constant  $E(m)$  to a linear function for  $E(m)_\lambda$  that increased at a rate of 40%/μm resulted in a 50 K increase in measured temperature (i.e., <3% on a measured temperature of 1700 K), and a 30% decrease in the estimated soot concentration [16]. Additionally, the soot concentration varies inversely with the absolute magnitude of  $E(m)$ . Therefore, the soot volume fraction is much more sensitive to the selection of  $E(m)$  than the temperature. For the present measurements, a constant  $E(m)$  function with a magnitude of 0.274 is assumed. This is consistent with the results of Krishnan et al. [20]. Modeling of the flame emission using the methods described in [16] shows that attenuation of emission by soot introduces only a small error in the measurements (i.e., <2%) for even the highest soot loadings observed in this flame. This result may seem surprising considering that soot volume fractions of 100 ppm have been measured in this flame; however, light attenuation is a function of the product of the soot concentration and the absorp-

tion path length. Although soot concentrations are an order of magnitude larger than those observed in the familiar Gülder or Santoro flames, e.g., [16,22], the flame diameter is much smaller and decreases with increasing pressure. Since the modeled correction is small no attenuation correction is applied. The overall uncertainty in the SSE temperature measurements is estimated to be 3.5% (95% confidence interval). This uncertainty is dominated by the uncertainty of the spectral shape of the refractive index function  $E(m)$ . The uncertainty of the SSE soot volume fraction measurements is estimated to be 35 to 40% (95% confidence interval). This uncertainty is dominated by uncertainty of the soot temperature measurements. A more detailed discussion of the error analysis for the SSE diagnostic can be found in [23].

The line-of-sight attenuation diagnostic is a simplified version of the 2D LOSA diagnostic described in [24]. In LOSA, a line-of-sight measurement is made of the intensity of a small light beam transmitted through a flame. When divided by a measurement of the intensity of the beam transmitted along the same path without the flame present, the transmissivity of the given chord through the flame can be determined. A series of transmissivity measurements at a given height in the flame can be inverted to obtain radially resolved extinction coefficients from which soot volume fraction can be determined. The optical layout for the LOSA measurements is included in Fig. 5. Light from a mercury arc lamp is first focused onto a 50-μm pinhole. Light transmitted through the pinhole is modulated using a chopper wheel and imaged at the center plane of the burner with a 1.5:1 demagnification at a speed of  $f/19$ . Knife-edge scans of the lamp beam at the burner center show the beam width to be less than 40 μm across the diameter of the burner nozzle. A collection lens downstream of the burner refocuses the transmitted light from the lamp onto a photodiode detector coupled to a lock-in amplifier. The collection lens is large (i.e., 100 mm diameter) to accommodate beam steering of the light transmitted through the flame, which becomes quite pronounced at 4 MPa. A glass plate located between the imaging lens and the chamber reflects a portion of the lamp light onto a second photodiode which is used to normalize the signal for any temporal variation in

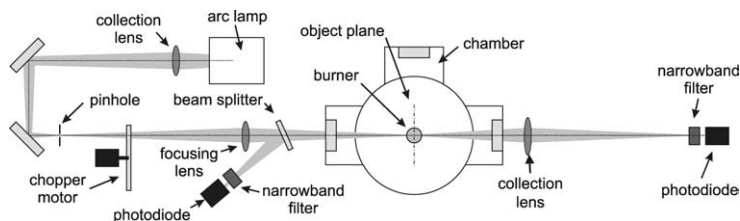


Fig. 5. Schematic of the line-of-sight attenuation diagnostic.

the lamp intensity. Both photodiodes are filtered with 830-nm narrow band filters. For each measurement height, two scans are required, one with the flame lit and the second with the flame extinguished. The method used to calculate soot volume fraction measurements from line-of-sight transmissivity measurements is described in [24]. For consistency,  $E(m) = 0.274$  was also used for the LOSA calculations. The uncertainty of the LOSA soot volume fraction measurements is estimated to be 20 to 30% (95% confidence interval). The uncertainty is dominated by the uncertainties in the magnitude of  $E(m)$  and the contribution of scatter to light attenuation measurements. A more detailed discussion of the error analysis for the LOSA diagnostic can be found in [23].

SSE and LOSA measurements were obtained in flames at pressures of 0.5, 1.0, 2.0, and 4.0 MPa. Constant mass-flow rates of methane and air of 0.55 mg/s and 0.4 g/s, respectively, were maintained at all pressures. For each pressure, measurements were obtained at height increments of 0.5 mm from the base to the tip of the flame and at horizontal increments of 50  $\mu\text{m}$ . Here, plots of spatially resolved soot volume fraction and temperature are reported only for height increments of 1.0 mm.

### 3. Results and discussion

Images of the 0.66 mg/s methane flame over a pressure range from 0.5 to 8.0 MPa are presented in Fig. 3. It is clear that the shape of the flame changes dramatically with increasing pressure. At atmospheric pressure, the flame has a bulbous appearance and is wider than the exit diameter of the burner nozzle. The presence of soot is limited to the region near the tip of the flame. As pressure increases, the flame narrows and the visible luminosity dramatically increases, suggesting that the soot zone extends down toward the rim of the burner. At all higher pressures, soot emissions dominate the visible flame appearance. The height of the flames increase gradually as pressure increases from 0.5 to 2 MPa and then decrease with further increases in pressure. These trends are consistent with observations by Miller and Maahs [12] for a 0.46 mg/s methane flame at pressure between atmospheric and 5.0 MPa; however, in [12], the peak flame height was observed to occur at a pressure of 1 MPa in contrast to the peak height at 2.0 MPa in the present work. Further measurements of flame height were obtained for the 0.55 mg/s methane flame. For this flame, the maximum flame height was observed at  $P = 1.0$  MPa, which is consistent with the results of Miller and Maahs [12], and suggests that the relationship between maximum flame height and pressure is also a function of fuel flow rate.

Soot volume fraction measurements are included in Fig. 6, for pressures of 0.5, 1.0, 2.0, and 4.0 MPa. SSE and LOSA measurements are presented in the same figure to allow direct comparison of the results. For both methods, scans across the entire flame diameter were performed; however, only averages from the left and right side scans are presented in the figure. The soot forms first in an annular band near the burner rim. Near the mid height of the flame, the annular distribution disappears and a peak soot concentration is observed on the flame centerline. From the curves, the significant contraction of the flame diameter with pressure is reflected in the location of the peaks in the radial profiles of soot volume fraction. Additionally, a dramatic increase of soot concentration with pressure is noted in the soot concentration curves.

It is observed that the overall agreement between the SSE and LOSA soot volume fraction measurements is good. The curves have very similar shape and locations of the peak soot concentrations correspond to within 10%. Differences in the peak soot concentrations are typically below 30% and therefore fall within the estimated experimental error in the techniques. The SSE curves often suggest higher values of soot concentration in the core of the flame. It is believed that this relates to a bias in the SSE measurements in the core of the flame due to the inclusion of background radiation in the SSE signal. Differences in the soot volume fraction measurements for the two diagnostics are highest at the tip of the flame. This may result from high gradients of the soot concentration along the  $z$  axis at the tip of the flame and noise in the measurements due to flame tip flicker. There are several other sources that might explain the differences between the measurements from the two diagnostics. First, the LOSA diagnostic measures the soot extinction coefficient, which includes both absorption and scatter, rather than the soot absorption coefficient from which soot volume fraction is properly determined. Consequently, extinction measurements will tend to consistently overestimate values of soot volume fraction. Direct measurement of light scatter or of soot morphology would allow improved LOSA soot volume fraction measurements. Second, since the values of soot volume fraction measured using SSE are coupled to the measured soot temperatures, any errors in measured temperatures will lead to errors in soot volume fractions. For example, pyrometry temperature measurements are inherently biased to give high mean temperatures and low mean soot concentrations when there is a temperature gradient in the measurement control volume. The uncertainties in temperature will be discussed further in the context of the temperature measurements.

Fig. 6 illustrates that the flame narrows with increasing pressure. Theoretical analysis suggests that

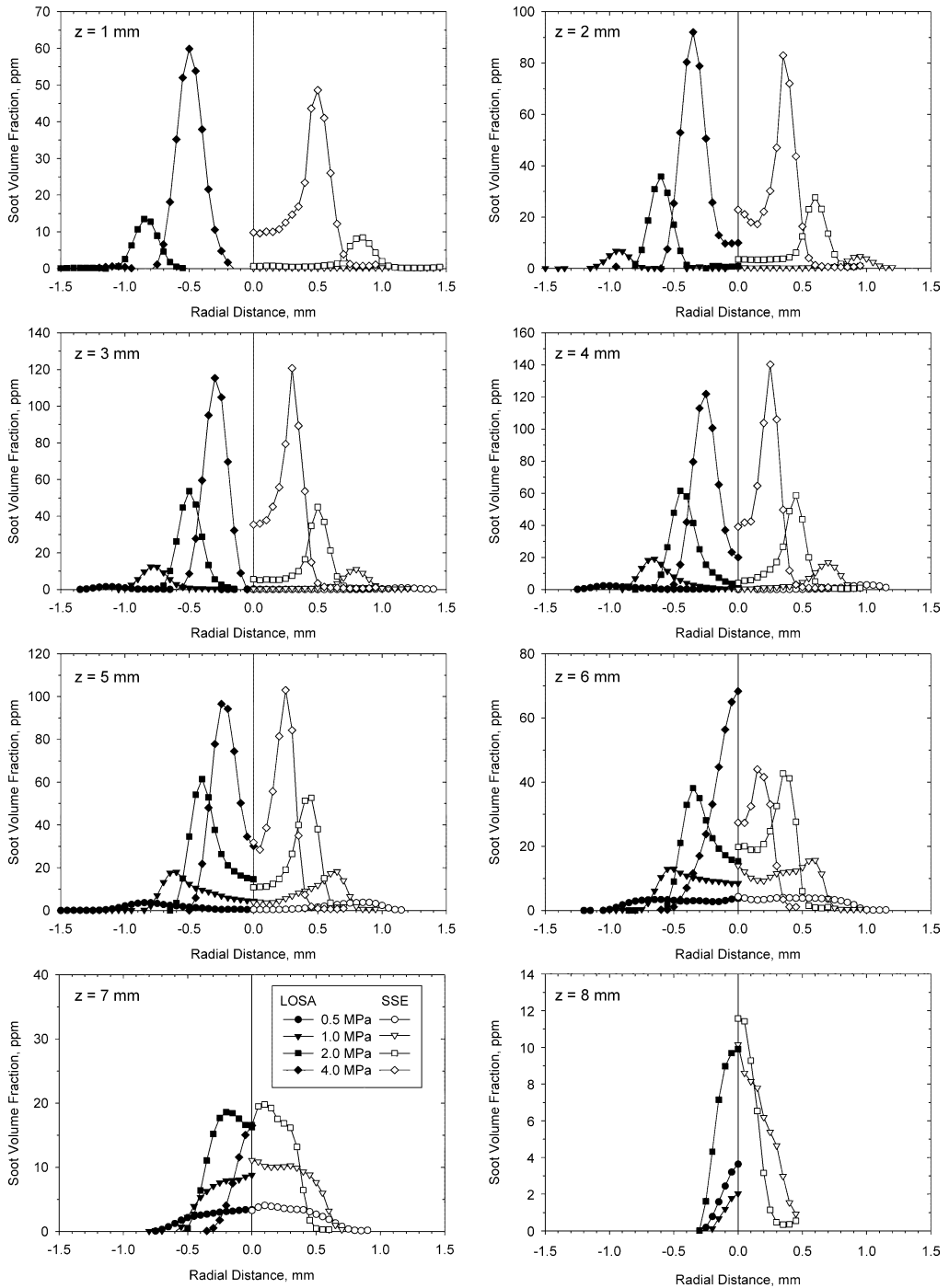


Fig. 6. LOSA (left, full symbols) and SSE (right, open symbols) measurements of soot concentration for  $P = 0.5, 1.0, 2.0,$  and  $4.0$  MPa at heights of 1 to 8 mm. The methane flow rate is  $0.55$  mg/s and the air flow rate is  $0.4$  g/s. Note: not all pressures displayed at all heights.

the height of diffusion flame fed by fuel at a constant mass flow rate is invariant with pressure [13,25]. This prediction is approximately true over the pressure range studied here. Residence time is also thought

to be independent of pressure [13] which can only be possible if the flame area decreases inversely with pressure (neglecting the effects of air entrainment or changes in the shape of the temperature distribution).

The cross-sectional area of the flame,  $A_{CS}$ , was measured based on the radial location of the outer edges of the sooting region at each measurement height. It decreases with pressure as  $A_{CS} \propto P^{-n}$ , where  $n = 1.0 \pm 0.1$ . Although the observed value of  $n$  is consistent with the above argument, it is approximately double the value suggested by Glassman [26]. Nonetheless, based on the data in this study, residence time is assumed to be independent of pressure, and measurements at the same height above the burner exit are deemed comparable.

Both SSE and LOSA measurements indicate that the maximum soot volume fraction increases as  $f_{v_{max}} \propto P^2$  over the pressure range of 0.5 to 2.0 MPa. This is consistent with the limited results of Lee and Na [15] for an ethylene flame. Comparing the results at 2.0 and 4.0 MPa, the rate of increase in soot volume fraction drops to  $f_{v_{max}} \propto P^{1.2}$ , suggesting that there is a change in the sensitivity of the flame-sooting propensity to pressure at pressures above 2.0 MPa. Possible reasons for the diminished sensitivity could be a change in the soot formation mechanism, a change in residence time, or some phenomena related to high radiative heat loss or depleted quantities of soot growth species at these pressures.

As expected, soot volume fraction increases with increasing pressure since the flame is narrowing, suggesting that all species are at higher concentrations. To quantify the sooting propensity of the flame at different pressures it is useful to calculate the percentage of total carbon converted to soot as a function of height. The mass flow rate of carbon, in the form of soot, can be determined through the relationship

$$\dot{m}_s(z) = v_z(z) \rho_s \int 2\pi r f_v(r, z) dr, \quad (2)$$

where  $v_z$  is the axial velocity and  $\rho_s = 1.8 \text{ g/cm}^3$  is the soot density. The axial velocity is estimated using the relationship  $v_z(z) = \sqrt{2az}$ , where  $a$  is an acceleration constant commonly assumed to be  $25 \text{ m/s}^2$  [13,27]. The percentage of carbon in the fuel converted to soot is simply  $\eta_s = \dot{m}_s / \dot{m}_c$ , where  $\dot{m}_c$  is the carbon mass-flow rate at the nozzle exit. The results of this calculation are included in Fig. 7. Peak carbon conversion occurs at a height of about 5.5 mm above the burner nozzle for pressures of 0.5 and 1.0 MPa, 5 mm for a pressure of 2.0 MPa, and 4 mm for a pressure of 4.0 MPa. Up to the point of peak carbon conversion, the curves of carbon conversion with height are approximately linear and the slopes increase with increasing pressure. Extrapolation of the curves in Fig. 6 to the height corresponding to zero carbon conversion to soot shows that soot inception moves closer to the burner as pressure increases. This suggests that fuel pyrolysis and soot nucleation are enhanced at higher ambient pressure. A plot of

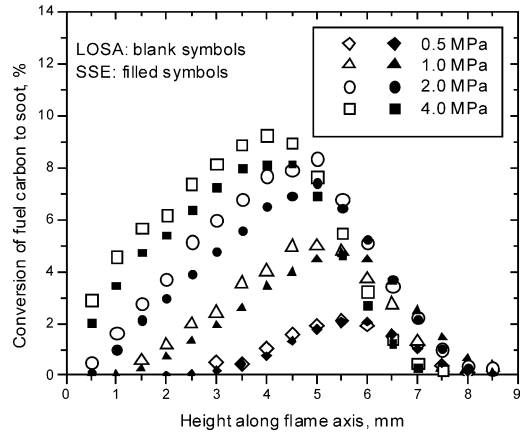


Fig. 7. Percentage conversion of carbon from fuel to soot as a function of axial location for  $P = 0.5, 1.0, 2.0,$  and  $4.0$  MPa.

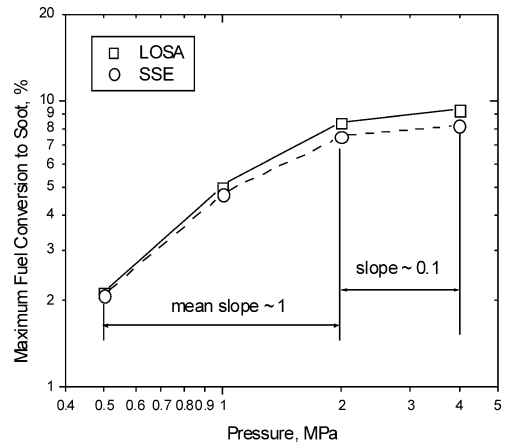


Fig. 8. Maximum percentage conversion of carbon from fuel to soot as a function of pressure.

maximum percentage conversion of carbon to soot as a function of pressure is included in Fig. 8. It is observed that  $\eta_s \propto P^n$ , where  $n = 1$  for pressures ranging between 0.5 and 2.0 MPa and  $n = 0.1$  for the pressure range of 2.0 to 4.0 MPa. Thus even when the impact of flame narrowing is integrated out, it is shown that soot formation is enhanced by pressure. However, at pressures between 2.0 and 4.0 MPa, the sensitivity is quite low and it is speculated that the values of maximum carbon conversion to soot could begin to drop at pressures above 4.0 MPa. Further measurements at pressures above 4.0 MPa are needed to better understand the sooting trends. It is noted that in this methane flame, the carbon conversion to soot peaks at about 9% compared to 40–50% observed by Flower and Bowman in an ethylene flame [13].

To compare the current results with those of Flower and Bowman [13] and Lee and Na [15], line integrals of the soot concentration profiles were cal-

culated, i.e., Eq. (2). It is found that the maximum line integrated soot volume fraction,  $f_{v\text{line}}$ , varies as  $f_{v\text{line}} \propto P^n$ , where  $n = 1.3$  for  $P = 0.5$  to 2.0 MPa and  $n = 0.9$  for  $P = 2.0$  to 4.0 MPa. It is noted that for the lower pressure range, the correlation agrees with results of Flower and Bowman [13] and Lee and Na [15] and that the agreement with the carbon conversion rate is fair; however, for the 2.0 to 4.0 MPa range, line-of-sight integrated measurements do not capture the dramatic change in the soot propensity of the flame which is observed with the peak soot conversion calculation described above. It is therefore concluded that line-of-sight integrated soot volume fraction values can be a misleading measure of the sooting tendencies of annular flames.

Measured soot temperature for pressures of 0.5, 1.0, 2.0, and 4.0 MPa are plotted in Fig. 9. Since the measurements are based on measurements of soot emission, temperatures can only be determined in locations where sufficient soot exists to provide a resolvable signal. This typically occurs at radial locations centered about the zones of peak soot volume fraction. From previous characterization of the SSE diagnostic [16], temperatures are known to decrease at the outer edges of the annuli earlier than would be predicted by flame models or other experimental diagnostics, thus underpredicting the peak temperature in the reaction zone. It is believed that this fall off is caused by errors introduced through the inversion algorithm when inverting the rapidly decreasing line-of-sight emission intensities at the edge of the flame. In the core of the flame, temperatures can also be inaccurate when soot volume fractions are low relative to peak soot volume fractions in the annulus. Consequently, the temperature plots provided here have been limited to regions centered about the soot annuli. This is justified by the fact that the agreement between soot volume fraction measurements using SSE and LOSA in these regions is good and requires an accurate estimation of the soot temperature. The radial temperature profiles are qualitatively similar to those observed in atmospheric pressure nonpremixed flames [16,28]. It is believed that the increased uncertainties in temperatures in the core of the flame and on the outside of the soot annulus may be linked to optical limitations and beam steering when the SSE diagnostic is applied in such a narrow flame. The greatest disagreement between LOSA and SSE measurements is observed in the core of the flame. Here, the uncertainty in temperature measurements limits the accuracy of the SSE soot volume fraction measurements. It is noted that the temperature curves are repeatable, within 2%, including any anomalous temperature values discussed above.

The temperature plots in Fig. 9 show steep radial temperature gradients across the soot annulus and a

general axial increase in temperature. The rate of temperature increase with axial position increases with increasing pressure; however, the overall temperature drops with increasing pressure, most significantly in the lower half of the flame. Using the temperature plots, radial temperature gradients were calculated and are plotted in Fig. 10. The gradients are initially high in the lower part of the flame and then drop slightly before climbing and peaking in proximity to the mid height of the flame. In the upper half of the flame, radial temperature gradients decrease and eventually become negative as the peak temperature migrates to burner centerline. The magnitude of the gradient increases with increasing pressure and the location of the first minima of the radial temperature gradient shifts toward the burner base. In the middle of the flames, the peak gradient is around 400 K/mm at  $P = 0.5$  MPa and 1000 K/mm at  $P = 4.0$  MPa, although the measured gradients are much noisier at 4.0 MPa than at the lower pressures. This is most likely because fewer temperature points are available with which to calculate the gradients. Trends in the gradients are indicative of the dramatic narrowing of the flame observed for increasing pressure. They also contribute to the explanation of the observed lower temperatures in the lower half of the flame at higher pressures, since the rate of heat conduction from the soot annulus to the core of the flame scales with the temperature gradient. With higher gradients, energy is drawn from the reaction zone into the core of the flame.

To allow a more consistent comparison with the results of Flower [14], temperatures were calculated from line-of-sight emission measurements through the flame center. Fig. 11 includes a plot of these averaged temperatures as a function of height. Since the measurements are line of sight, they represent a soot concentration-weighted average temperature along a chord through the flame and should correspond closely to the peak soot volume fraction temperatures. The data are indeed very close in trend to the temperatures found for the peak soot volume fractions obtained from examination of Figs. 6 and 9, though higher by about 50 K. The results are similar to those of Flower [14] in that a high-temperature region is observed near the base of the flame. This high-temperature region likely exists because of preheating of reactants from the nozzle and from the flame reaction zone which resides concentrically outside of the soot annulus. The temperature minima move toward the burner outlet with increasing pressure. This correlates well with the carbon conversion to soot which begins closer to the tip of the burner with increasing pressure. Additionally, temperature increases with height from a minimum value near the burner outlet. The rate of increase increases with pressure. The

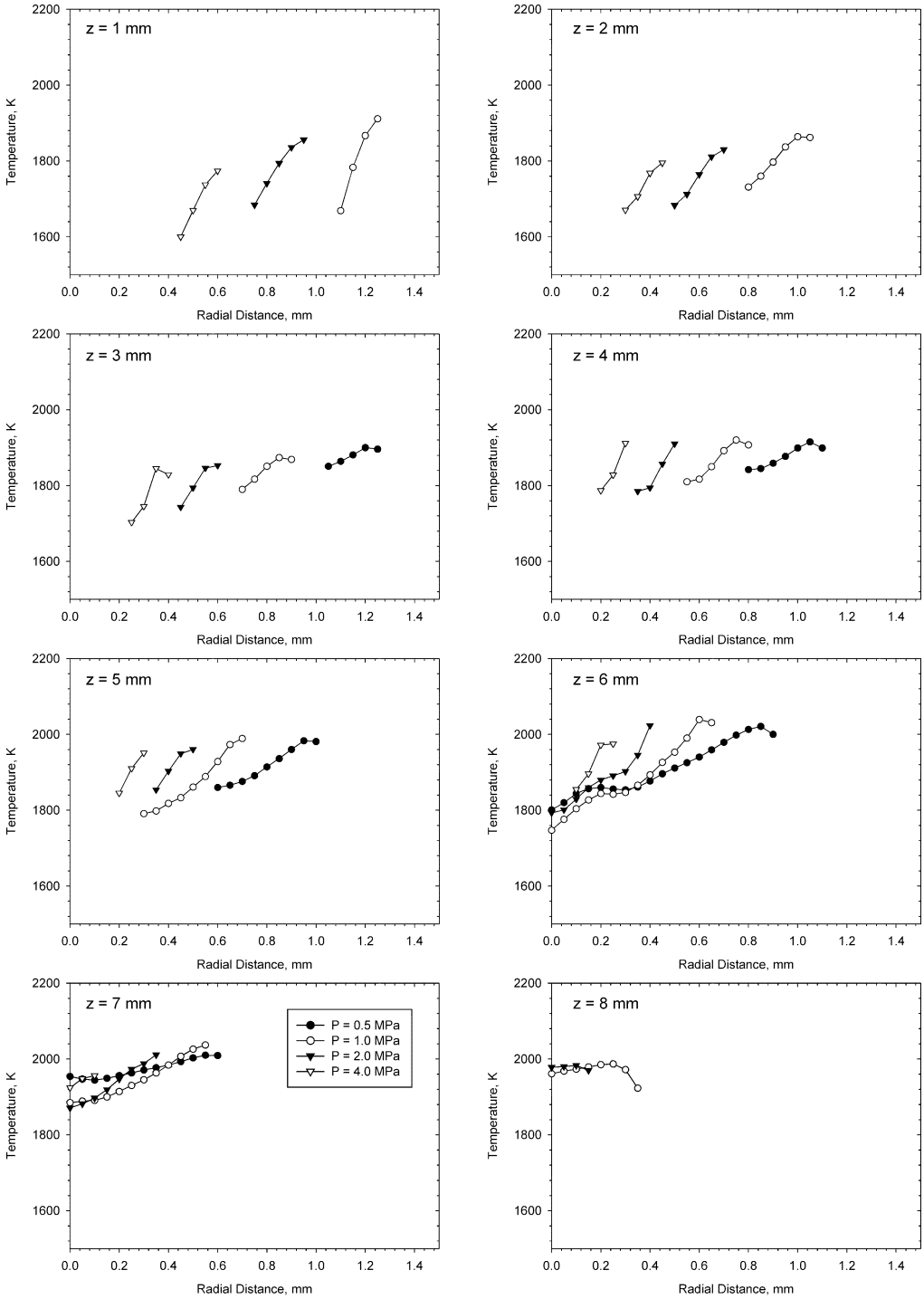


Fig. 9. SSE measurements of soot temperature for  $P = 0.5, 1.0, 2.0,$  and  $4.0$  MPa at heights of 2 to 8 mm. Note: not all pressures displayed at all heights.

range of observed temperatures (i.e., the range from the minimum to maximum temperatures) increases with pressure from  $T = 100$  K at  $P = 0.5$  MPa to  $T =$

250 K at  $P = 4.0$  MPa. Finally, average temperatures drop with increasing pressure, though the effect is less pronounced in the upper half of the flame. In flames

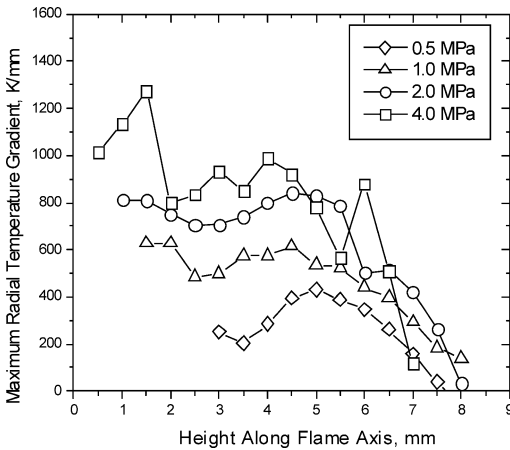


Fig. 10. Radial gradients of soot temperature as a function of axial location for  $P = 0.5, 1.0, 2.0,$  and  $4.0$  MPa.

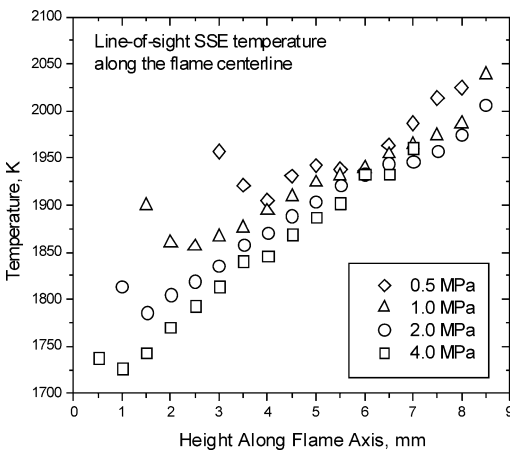


Fig. 11. Line-of-sight emission averaged soot temperature as a function of axial location for  $P = 0.5, 1.0, 2.0,$  and  $4.0$  MPa.

reported by Flower [14], the average soot particle temperature of line-of-sight measurements through the flame center decreases with height in the upper half of the flame except at a pressure of 0.1 MPa. The reason for this behavior is that all flames, except that at 0.1 MPa, were sooting flames; therefore, soot is not completely oxidized and it escapes from the flame tip. In flames studied in the present work no soot escapes from the flame tip; therefore, all soot is oxidized within the visible yellow/orange flame region. For this reason, the average temperatures shown in Fig. 11 display an increase with downstream distance along the flame axis. The temperature curves converge at the tip of the flame in the current study. This was not observed in the flames of Flower [14] due to the cessation of soot oxidation. Finally, the temperature measurements in the current experiment are about 200 K higher than those in [14]. This may

relate to differences in fuel, soot loading, radiant heat loss, and pressure considered in these studies.

Lower in the flame and at higher pressures there seem to be three factors affecting the local temperatures: (a) a nontrivial amount of carbon is converted to soot, thus lowering the heat released by oxidation of the fuel, (b) higher soot concentrations lead to higher radiative heat losses from the flame, and (c) enhanced heat conduction to the core of the flame reduces the temperature in the soot annulus. As a result, temperatures in Fig. 11 show a definite and significant decrease with increasing pressure at axial locations up to 4–5 mm. At locations higher than 4–5 mm, soot concentrations start decreasing rapidly due to soot oxidation (Fig. 7). The heat release resulting from oxidation of soot at higher pressures keeps local temperatures close to the temperatures seen in lower pressure cases, as shown in Fig. 11. Also, the local radiation heat loss is less pronounced due to lower soot concentrations (as well as lower temperatures). Finally, radial temperature gradients are reduced, suggesting that the core of the flame has been heated by the soot annulus. The interplay of these phenomena seems to determine the temperature trends observed in Fig. 11. This explanation also resolves the question of how, despite the mild temperature increases expected with increasing pressure, observed soot temperatures were lower at higher pressures.

#### 4. Conclusions

The work presented here represents a significant addition to the available database of information on soot formation tendencies as a function of pressure for nonpremixed laminar flames. For the first time spatially resolved soot volume fraction measurements have been made in laminar nonpremixed flames over the pressure range of 0.5 to 4.0 MPa. Flame cross-sectional area is observed to decrease with pressure as  $A_{CS} \propto P^{-n}$ , where  $n = 1 \pm 0.1$ . SSE and LOSA measurements of soot volume fraction agree within 30% and show that the peak soot concentration varies as  $f_{v,max} \propto P^n$ , where  $n = 2$  for  $P = 0.5$  to 2.0 MPa and  $n = 1.2$  for  $P = 2.0$  to 4.0 MPa. Peak carbon conversion to soot mass increases with pressure as  $m_s \propto P^n$ , where  $n = 1$  for  $P = 0.5$  to 2.0 MPa and  $n = 0.1$  for  $P = 2.0$  to 4.0 MPa. It is apparent from these correlations that soot formation is initially enhanced by increases in pressure above atmospheric but that it becomes less sensitive to pressure above 2.0 MPa. More pressures in this range should be studied to better quantify trends for further increases in pressure. The soot measurements, when appropriately transformed, are consistent with the line-averaged measurements of Flower and Bowman [13] and Lee and Na [15];

however, based on the results, it is concluded that line-averaged soot volume fraction measurements do not provide a clear picture of soot formation trends.

Soot temperature measurements show that the overall temperature decreases with increasing pressure; however, the level of decrease drops with increasing height in the flame. Low down in the flame temperatures are about 150 K lower at 4.0 versus 0.5 MPa. In the upper half of the flame the differences between temperatures in the 0.5 and 4.0 MPa flames reduce to 50 K. Radial temperature gradients of 400 K/mm at  $P = 0.5$  MPa up to 1200 K/mm at  $P = 4.0$  MPa are observed in the soot annulus. The decrease in flame temperature with increased pressure is believed to occur because of a combination of several factors. First, the significant amount of carbon converted to soot reduces the energy available from oxidation of the fuel. Secondly, this soot leads to significant heat loss from the flame by radiation to the environment. Finally, heat conduction to the core of the flame is much higher in the highly sooting, higher pressure flames. These combined phenomena contribute to the convergence of temperature data high up in the flame. Line-averaged temperature results show trends similar to those of Flower in the lower half of the flame [14], though the temperatures from the present work are about 200 K higher. Differences relate to the different fuels used, the relative soot loadings in the flames, radiant heat losses, and the cessation of soot oxidation in the flames of [14].

### Acknowledgments

This work was performed at the National Research Council of Canada and supported in part by the AFTER POL of the Canadian Government's PERD program. Funding for K.A. Thomson has been provided in part by a Carl A. Pollock Fellowship from the University of Waterloo, research grants from the Natural Sciences and Engineering Research Council (NSERC) of Canada, as well as a Graduate Student Supplement Scholarship from the National Research Council of Canada.

### References

[1] U.S. EPA, Fed. Reg. EPA/600/8-90/057F, 2002.

- [2] J. Ferin, G. Oberdörster, D.P. Penney, S.C. Soderholm, R. Gelein, H.C. Piper, *J. Aerosol Sci.* 21 (1990) 381–384.
- [3] G. Oberdörster, J. Ferin, G. Finkelstein, P. Wade, N. Corson, *J. Aerosol Sci.* 21 (1990) 384–387.
- [4] U.S. EPA, Fed. Reg. 66 (12) (2001) 5001–5050.
- [5] H. Böhm, C. Feldermann, T. Heidermann, H. Jander, B. Luers, H.G. Wagner, *Proc. Combust. Inst.* 24 (1992) 991–998.
- [6] S. Hanisch, H. Jander, T. Pape, H.G. Wagner, *Proc. Combust. Inst.* 25 (1994) 577–584.
- [7] T. Heidermann, H. Jander, H.G. Wagner, *Phys. Chem. Chem. Phys.* 1 (15) (1999) 3497–3502.
- [8] R.V. Ravikrishna, D.D. Thomsen, N.M. Laurendeau, *Combust. Sci. Technol.* 157 (2000) 243–261.
- [9] C.G. Fotache, T.G. Kreutz, C.K. Law, *Combust. Flame* 110 (4) (1997) 429–440.
- [10] A.M. Saur, F. Behrendt, E.U. Franck, *Ber. Bunsenges. Phys. Chem.* 97 (7) (1993) 900–908.
- [11] C.H. Sohn, S.H. Chung, *Combust. Flame* 121 (1–2) (2000) 288–300.
- [12] I.M. Miller, H.G. Maahs, NASA Technical Paper TN D-8407, 1977.
- [13] W.L. Flower, C.T. Bowman, *Proc. Combust. Inst.* 21 (1986) 1115–1124.
- [14] W.L. Flower, *Combust. Flame* 77 (1989) 279–293.
- [15] W. Lee, Y.D. Na, *JSME Int. J. Ser. B* 43 (4) (2000) 550–555.
- [16] D.R. Snelling, K.A. Thomson, G.J. Smallwood, Ö.L. Gülder, E.J. Weckman, R.A. Fraser, *AIAA J.* 40 (9) (2002) 1789–1795.
- [17] C.J. Dasch, *Appl. Opt.* 31 (8) (1992) 1146–1152.
- [18] Ü.Ö. Köylü, G.M. Faeth, *J. Heat Transfer* 115 (1993) 409–417.
- [19] F. Xu, G.M. Faeth, *Combust. Flame* 125 (1–2) (2001) 804–819.
- [20] S.S. Krishnan, K.-C. Lin, G.M. Faeth, *J. Heat Transfer* 122 (2000) 517–524.
- [21] K.C. Smyth, C.R. Shaddix, *Combust. Flame* 107 (3) (1996) 314–320.
- [22] R.J. Santoro, H.G. Semerjian, *Proc. Combust. Inst.* 20 (1984) 997–1006.
- [23] K.A. Thomson, PhD thesis, University of Waterloo, Waterloo, Canada, 2004.
- [24] D.R. Snelling, K.A. Thomson, G.J. Smallwood, Ö.L. Gülder, *Appl. Opt.* 38 (12) (1999) 2478–2485.
- [25] F.G. Roper, *Combust. Flame* 29 (3) (1977) 219–226.
- [26] I. Glassman, *Proc. Combust. Inst.* 27 (1998) 1589–1596.
- [27] F.G. Roper, C. Smith, A.C. Cunningham, *Combust. Flame* 29 (3) (1977) 227–234.
- [28] R.J. Santoro, T.T. Yeh, J.J. Horvath, H.G. Semerjian, *Combust. Sci. Technol.* 53 (2–3) (1987) 89–115.